Journal of Dynamics, Monitoring and Diagnostics, 2024, 3, 297-310
https://doi.org/10.37965/jdmd.2024.555

ISTP
RESEARCH ARTICLE

Non-Smooth Self-Excited Vibration of a Novel Dynamical Model for a Disc Brake

Ningyu Liu,[1] Huajiang Ouyang,[2,3] Yiqiang Fu,[4] and Wei-Hsin Liao[1]

[1]Department of Mechanical and Automation Engineering, The Chinese University of Hong Kong, Shatin, NT, Hong Kong, China

[2]School of Mechanical Engineering, Southwest Jiaotong University, Chengdu, China

[3]School of Engineering, University of Liverpool, Liverpool, UK

[4]Department of Mechanical Engineering, The Hong Kong Polytechnic University, Hung Hom, Hong Kong, China

(Received 03 June 2024; Revised 08 September 2024; Accepted 23 September 2024; Published online 23 September 2024)

Abstract: This paper proposes a new dynamic model for the study of friction-induced self-excited vibration of a disc brake system, where the pad's motions in both radial and circumferential/tangential directions are included, which is in stark contrast to the previous studies that normally consider the pad's motion in the tangential/circumferential direction only. The non-smooth dynamics of the system including three different states of motion, i.e., stick, slip and separation, is investigated. Both the linear stability analysis and the transient dynamic analysis are performed. The numerical results in the linear stability analysis indicate that the inclusion of pad's radial motion in the present brake model significantly expands the ranges of operating parameters for dynamic instability than the brake model with only circumferential/tangential motion for the pad. For the transient dynamic analysis, two different methods, i.e., the time integration method and the shooting method, are employed for the calculation of steady-state response. The accuracy and efficiency of the shooting method are subsequently examined. The numerical results show rich bifurcation behaviours of the steady-state response in the present brake model with the variations of brake pressure N_0 and disc speed Ω, and that k_{ir} (the stiffness of the inclined spring in the radial direction) is a key parameter for controlling the occurrence of chaotic vibration in the system.

Keywords: friction-induced vibration; linear stability analysis; non-smooth; shooting method; transient dynamic analysis

I. INTRODUCTION

Brake noise is a major issue in the automobile industry today, which may cause discomfort to passengers and be perceived as a quality problem, thereby pushing up the warranty cost and impacting the brand reputation [1–3]. Because of its impact and scientific intricacy, brake noise has long been a research hotspot for engineers and researchers.

The vibration caused by the pad-disc frictional contact in the braking process has been acknowledged as the main reason for automobile brake noise [4], namely, brake noise is in essence a problem of friction-induced vibration. Four main mechanisms have been put forward to explain the occurrence of friction-induced vibration in mechanical systems; they are: the negative friction slope [5], the stick-slip motion [6], the sprag-slip instability [7] and the mode-coupling instability [8]. Apart from the four principal mechanisms above, there are other mechanisms proposed for the friction-induced vibration in specific systems. The destabilizing effects of the friction force as a follower force or a moving load in the disc brake systems were analysed [9–11]. Kinkaid *et al.* [12] found the change of direction of the friction force could excite vibration in a planar frictional system.

A number of studies have been devoted to the dynamic behaviours, e.g., bifurcations, chaos, non-stationary effect, etc, of the friction-induced vibration in the brake system, so as to reveal the properties of brake noise. Wu *et al.* [13] studied the self-excited vibration in the stern bearing of the underwater vehicle and its stick-slip phenomenon. Von Wagner *et al.* [14] proposed a 2-DoF brake model involving a wobbling disc and analysed its stability behaviour. Kang *et al.* [15,16] used the finite element models of the pad-disc system for investigation of the dynamic instability in disc brakes. Li *et al.* [17] found the non-stationary dynamic characteristic of the brake system. Liu and Ouyang [18] investigated the bifurcation behaviours of FIV of a 5-DoF dynamic model with multiple types of nonlinearities. Wei *et al.* [19,20] established 2-DoF and 3-DoF dynamic models of a brake system and observed the bifurcation and chaotic behaviours of system responses. Some works focused on the accurate models of the complex friction phenomena and their effects on the system dynamics [21–23].

The existing studies on the friction-induced vibration in brake systems usually assume a constant direction of relative motion and friction force, i.e., the circumferential direction, and thus only the vibration in the circumferential direction is investigated when in-plane vibration of a brake system is concerned. Nevertheless, because of factors such as manufacturing errors, external disturbances, flexible connections, etc, relative vibration of a brake component may happen in any direction in the three-dimensional space and therefore causes the direction of friction force to vary with time, which then further complicates the dynamics of a

Corresponding authors: Huajiang Ouyang; Wei-Hsin Liao (e-mails: h.ouyang@liverpool.ac.uk; whliao@cuhk.edu.hk).

brake system. In view of the above, it is essential to consider the oscillations of brake components in the directions apart from the circumferential direction, e.g., the radial and the vertical (transverse) directions, and the direction of the friction force to be unknown a priori and to be determined with the dynamics of the brake system. There have been investigations of the vibration of mechanical systems under the friction force with a state-dependent direction. Antali and Stepan [24] examined the three-dimensional dynamics of a rigid body in sliding or rolling contact with a rigid plane. Ma and Wang [25] dealt with planar multiple-contact problems subjected to unilateral and bilateral kinetic constraints. Sinou *et al.* [26,27] studied the self-excited vibration of a non-smooth dynamical system with planar frictional contact. Menq *et al.* [28] put forward an approximate method for analysing the dynamic responses of structures having a two-dimensional frictional constraint. With the aim of enhancing the study of friction-induced-vibration problems in automobile brakes, we propose a novel dynamic model of a brake system including three-dimensional (circumferential, radial and vertical) oscillations of the brake pad and planar motion of the brake disc in this paper.

There are two main categories of methods for the analysis of friction-induced vibration in brake systems, i.e., the complex eigenvalue analysis (CEA) and the transient dynamic analysis (TDA). The linear complex eigenvalue approach is often employed for the stability analysis of the steady sliding state [29–34]. It can be used for the initial estimations of unstable modes which possibly lead to limit cycle vibration. The transient dynamic analysis is used to observe the dynamic behaviour of the system during the whole dynamic process, which enables acquiring the system behaviours in the steady state. The transient dynamic analysis can be performed by numerical integrations in the time domain from given initial conditions [35–38]. However, these numerical integrations are usually computationally expensive due to the non-smooth behaviours (i.e., the switches of states of motion including slip, stick and separation in the whole dynamic process) in the friction-induced-vibration problems. Alternative methods have been developed for efficient calculations of steady-state limit cycles of the nonlinear self-excited vibration in frictional systems, e.g., the constrained harmonic balance method [39], the orthogonal collocation method [40], the shooting method [41]. In this paper, both CEA and TDA will be performed on the dynamic system in question. In terms of TDA, both the method of numerical integration and the shooting method will be employed, and the accuracy and efficiency of these two methods will be examined.

II. THE DYNAMICAL MODEL

The new dynamical model for a disc brake system consists of two parts, i.e., a rigid disc of mass M and rotational inertia I that models the brake disc, and a slider with mass m that models the brake pad that is at the radial distance of r_0 from the centre of the disc. The disc is constrained at the centroid by translational springs and dampers (k_{dx}, c_{dx} along the x axis and k_{dy}, c_{dy} along the y axis), and a rotational spring and damper ($k_{\mathrm{d}\psi}$, $c_{\mathrm{d}\psi}$), which model the flexible connections between the disc shaft and the disc. During vibration, the pad's motion in the radial and normal direction may become significant and therefore greatly affects the dynamics of the brake system. Therefore, the constraints that the brake pad is subjected to are modelled by the springs and dampers in both circumferential ($k_{\mathrm{p}\theta}$, $c_{\mathrm{p}\theta}$) and radial (k_{pr}, c_{pr}) directions. In either of the circumferential direction and the radial direction, there is an inclined spring ($k_{\mathrm{i}\theta}$ and k_{ir}, respectively) at 45° relative to the horizontal direction on the pad. Besides, there is a damper c_z on the pad in the vertical direction. The contact between the pad and the disc is assumed to be unilateral, and a linear spring k_z is used to model the contact stiffness. The three-view drawing of the brake system model is shown in Fig. 1.

Because of the translational motion of the disc and the pad's motion in the radial direction, the direction of the friction force usually will not be in the circumferential direction, rather, it varies with the system dynamics. The kinematics of the frictional contact of the pad and the disc during vibration is illustrated in Fig. 2, where axes $\mathbf{e}_x$ and $\mathbf{e}_y$ are fixed in space, O_1 is the centre of the disc, P_0 and P represent the initial position and the instantaneous position of the pad, respectively, $\mathbf{e}_{\mathrm{n}}$ represents the unit vector of the velocity of the disc at the contact point. The dynamic equations of the system are formulated as

$$\begin{cases} M\ddot{x} + c_{\mathrm{dx}}\dot{x} + k_{\mathrm{dx}}x = -\mathbf{F}_{\mathrm{f}} \cdot \mathbf{e}_x \\ M\ddot{y} + c_{\mathrm{dy}}\dot{y} + k_{\mathrm{dy}}y = -\mathbf{F}_{\mathrm{f}} \cdot \mathbf{e}_y \\ I\ddot{\psi} + c_{\mathrm{d}\psi}\dot{\psi} + k_{\mathrm{d}\psi}\psi = -R\mathbf{F}_{\mathrm{f}} \cdot \mathbf{e}_{\mathrm{n}} \\ m\ddot{r} + c_{\mathrm{pr}}\dot{r} + k_{\mathrm{pr}}r + \frac{1}{2}k_{\mathrm{ir}}r - \frac{1}{2}k_{\mathrm{ir}}z = -\mathbf{F}_{\mathrm{f}} \cdot \mathbf{e}_r \\ (r_0 + r)(m\ddot{\theta} + c_{\mathrm{p}\theta}\dot{\theta} + k_{\mathrm{p}\theta}\theta + \frac{1}{2}k_{\mathrm{i}\theta}\theta) - \frac{1}{2}k_{i\theta}z = -\mathbf{F}_{\mathrm{f}} \cdot \mathbf{e}_\theta \\ m\ddot{z} + c_z\dot{z} - \frac{1}{2}k_{\mathrm{ir}}r - \frac{1}{2}k_{\mathrm{i}\theta}r_0\theta + \frac{1}{2}(k_{\mathrm{ir}} + k_{\mathrm{i}\theta})z + N_0 = N \end{cases} \tag{1}$$

where x, y and ψ represent the planar translational motion and the rotational motion of the disc due to elastic constraints, and r, θ, z represent the planar motion and the vertical motion of the pad in the cylindrical coordinate

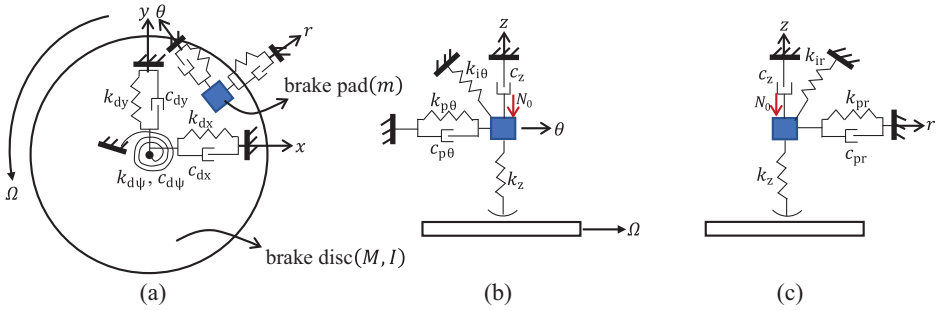

Fig. 1. The new brake system model: (a) top view, (b) circumferential view, (c) radial view.

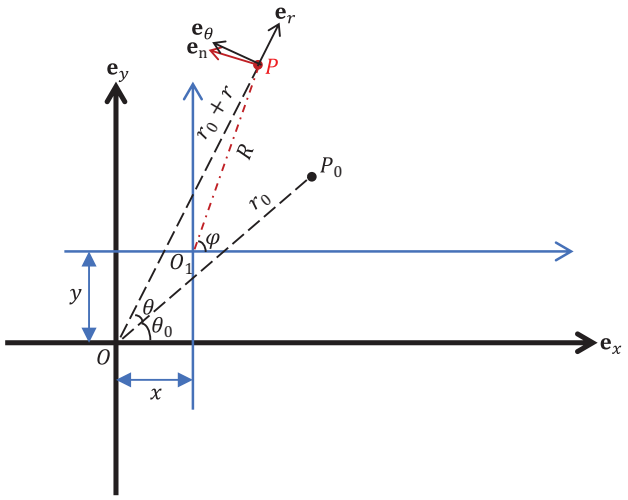

Fig. 2. The planar kinematics of the pad and the disc.

system. N_0 is the normal preload between the pad and the disc, $\mathbf{e}_n$ can be expressed as

$$\begin{aligned}\mathbf{e}_n &= -\sin\varphi\mathbf{e}_x + \cos\varphi\mathbf{e}_y \\ &= -\frac{(r_0+r)\sin(\theta_0+\theta)-y}{R}\mathbf{e}_x \\ &\quad + \frac{(r_0+r)\cos(\theta_0+\theta)-x}{R}\mathbf{e}_y\end{aligned} \tag{2}$$

R is the distance between the centre of the disc O_1 and the contact point P, which is

$$R=\sqrt{[(r_0+r)\cos(\theta_0+\theta)-x]^2+[(r_0+r)\sin(\theta_0+\theta)-y]^2} \tag{3}$$

The friction force between the pad and the disc is assumed to follow the Coulomb's law [42], i.e.,

$$\begin{cases}\mathbf{F}_f = -\mu_k N\frac{\mathbf{v}_r}{\|\mathbf{v}_r\|} & \|\mathbf{v}_r\|\neq 0 \\ \|\mathbf{F}_f\|\le \mu_k N & \|\mathbf{v}_r\|=0\end{cases} \tag{4}$$

where $N=-k_z z$, μ_k is the coefficient of friction, $\mathbf{v}_r$ is the relative velocity between the pad and the disc at the contact point, i.e.,

$$\mathbf{v}_r = \mathbf{v}^p - \mathbf{v}_c^d \tag{5}$$

where $\mathbf{v}^p$ and $\mathbf{v}_c^d$ represent the velocity of the pad and the velocity of the disc at the contact point, respectively, which can be obtained as

$$\mathbf{v}^p = \dot{r}\mathbf{e}_r + (r_0+r)\dot{\theta}\mathbf{e}_\theta \tag{6}$$

$$\mathbf{v}_c^d = \dot{x}\mathbf{e}_x + \dot{y}\mathbf{e}_y + (\Omega+\dot{\psi})R\mathbf{e}_n \tag{7}$$

and $\mathbf{e}_r$, $\mathbf{e}_\theta$ can be expressed by $\mathbf{e}_x$ and $\mathbf{e}_y$ as

$$\begin{bmatrix}\mathbf{e}_r\\ \mathbf{e}_\theta\end{bmatrix} = \begin{bmatrix}\cos(\theta_0+\theta) & \sin(\theta_0+\theta)\\ -\sin(\theta_0+\theta) & \cos(\theta_0+\theta)\end{bmatrix}\begin{bmatrix}\mathbf{e}_x\\ \mathbf{e}_y\end{bmatrix} \tag{8}$$

By substituting equations (2) and (6)–(8) into equation (5), it is derived that,

$$\mathbf{v}_r = v_x\mathbf{e}_x + v_y\mathbf{e}_y \tag{9}$$

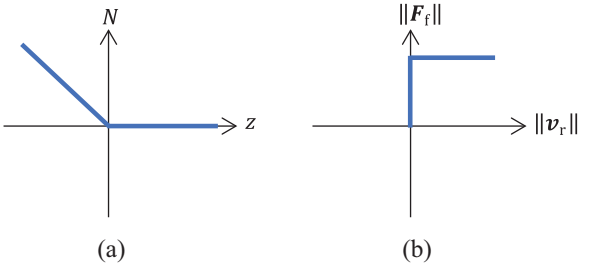

Fig. 3. The contact forces: (a) normal force, (b) friction force.

where

$$\begin{aligned}v_x &= (r_0+r)(\Omega+\dot{\psi}-\dot{\theta})\sin(\theta_0+\theta) \\ &\quad + \dot{r}cos(\theta_0+\theta) - \dot{x} - (\Omega+\dot{\psi})y, \\ v_y &= (r_0+r)(-\Omega-\dot{\psi}+\dot{\theta})\cos(\theta_0+\theta) \\ &\quad + \dot{r}sin(\theta_0+\theta) - \dot{y} + (\Omega+\dot{\psi})x\end{aligned}$$

By substituting equation (9) into equation $(4)_1$, the friction force between the pad and the disc when $\|\mathbf{v}_r\|\neq 0$ (i.e., the state of slip) is acquired. When $\|\mathbf{v}_r\|=0$ (i.e., the state of stick), however, the friction force serves as a reactive force to sustain the relative static state, and thus $\mathbf{F}_f$ will be determined by the dynamic equations of the system, i.e., equation (1). When $z>0$, the pad will separate from the disc, hence $N=0$, and $\mathbf{F}_f=\mathbf{0}$. The contact forces are illustrated in Fig. 3.

To summarize, the system may experience three distinct states of motion (slip, stick and separation) in the process of vibration, which are governed by three different sets of equations of motion.

III. STABILITY ANALYSIS

In this section, the Lyapunov stability of the equilibrium point of the system corresponding to a steady sliding state is analysed, which can be used as the estimation of the dynamic stability of the system, i.e., whether the self-excited vibration will happen or not in the steady state.

Firstly, the equilibrium point of the system is found as the solution of the nonlinear algebraic equations, which are acquired by setting the terms of acceleration and velocity in equation (1) as zero. Secondly, a linear dynamic system is constructed by linearizing the original dynamic equations of the system, i.e., equation (1), around each equilibrium point, namely,

$$\mathbf{M}_L\ddot{\bar{\mathbf{u}}} + \mathbf{C}_L\dot{\bar{\mathbf{u}}} + \mathbf{K}_L\bar{\mathbf{u}} = \mathbf{0} \tag{10}$$

where $\mathbf{u}=[x,y,\psi,r,\theta,z]^T$, $\bar{\mathbf{u}}=\mathbf{u}-\mathbf{u}_e$, in which $\mathbf{u}_e$ is an equilibrium point which represents the state of steady sliding and has a unique solution for a system. $\mathbf{M}_L=\mathrm{diag}(M,M,I,m,mr_0,m)$, while the entries in $\mathbf{C}_L$ and $\mathbf{K}_L$ are complicated because of the friction force and thus provided in the Appendix. According to the theory of second-order linear homogeneous ordinary differential equations, the solution of equation (10) can be written as

$$\bar{\mathbf{u}} = \boldsymbol{\varphi}e^{st} \tag{11}$$

where $\boldsymbol{\varphi}$ and s are the eigenvector and eigenvalue, respectively. By substituting equation (11) into equation (10), a quadratic eigenvalue equation is obtained,

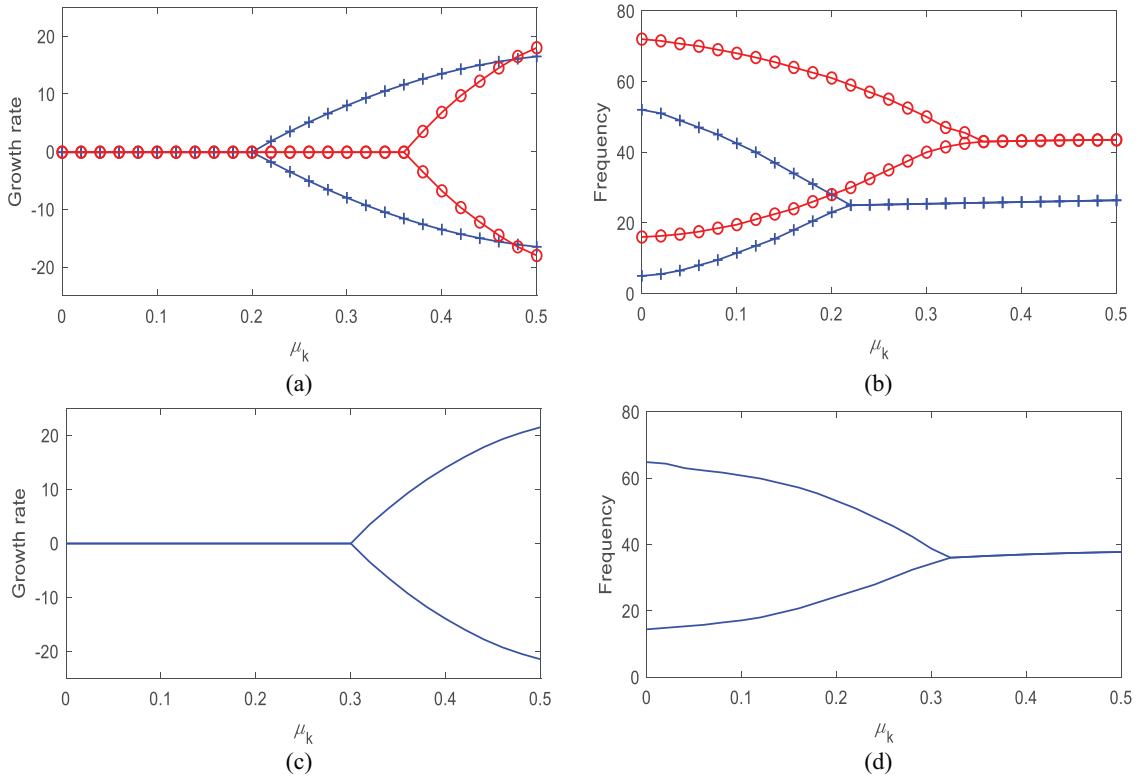

Fig. 4. The bifurcations of eigenvalues of the present model (a)(b) and when only the motion in the circumferential direction is considered (c)(d).

$$(s^2\mathbf{M}_L + s\mathbf{C}_L + \mathbf{K}_L)\boldsymbol{\varphi} = 0 \tag{12}$$

In terms of real matrices $\mathbf{M}_L$, $\mathbf{C}_L$ and $\mathbf{K}_L$ of order n, there are generally n pairs of conjugate complex eigenvalues that are solved from equation (12), i.e.,

$$s_{1,2}^j = \sigma_j \pm \omega_j \mathrm{i},\ j = 1,2,\ldots,6 \tag{13}$$

where $\mathrm{i} = \sqrt{-1}$ is the imaginary unit, σ_j and ω_j are the real part and imaginary part of the jth pair of eigenvalues, respectively, which indicate the growth rate and frequency of the jth mode in the response of the linearized system, therefore the stability of the equilibrium point of the frictional system that corresponds to steady sliding state can be evaluated by the signs of the real parts of eigenvalues. The positive real parts of at least one of the eigenvalues indicate an unstable equilibrium point and growing friction-induced self-excited vibration in the system when it is disturbed near that equilibrium point.

The Hopf bifurcation will happen in the system, i.e., the equilibrium point becomes unstable and limit-cycle vibration arises from the stable equilibrium point with the variations of parameters. To show the necessity of the inclusion of pad's motion radially, the results for the system with only pad's motion in the circumferential direction are also given in Fig. 4. Suppose that the structural parameters in the system are assigned the values listed in Table I, the bifurcations of the eigenvalues with the variation of μ_k at $N_0 = 50\mathrm{N}, \Omega = 5\mathrm{rad/s}$ for the present model and are presented. It is observed that two modes will be destabilized successively with the increase of μ_k in the present model, while only one unstable mode occurs in the system where the pad can only vibrate in the circumferential direction. Besides, the present model loses its stability at $\mu_k = 0.2$, which is significantly smaller than the needed coefficient of kinetic friction ($\mu_k = 0.31$) to cause instability in the system with pad's motion only in the circumferential direction.

The ranges of operating parameters Ω and N_0 corresponding to stable and unstable equilibrium points are shown in Fig. 5, in which the curves represent the boundaries between the ranges of parameter combinations leading to stable and unstable equilibrium points. As a comparison, the results when only the motion in the circumferential

Table I. The values of structural parameters in the system

M	m	I	k_{dx}	k_{dy}	$k_{d\psi}$	k_{pr}	k_{ir}
10 kg	1 kg	0.05 kg · m^2	10^4 N/m	10^4 N/m	10^4 N · m/rad	100 N/m	100 N/m
$k_{p\theta}$	$k_{i\theta}$	c_{dx}	c_{dy}	$c_{d\psi}$	c_{pr}	c_{ir}	$c_{p\theta}$
100 N/(m · rad)	100 N/(m · rad)	0.1 N · s/m	0.1 N · s/m	0.1 N · s · m/rad	10^{-3} N · s/m	10^{-3} N · s/m	10^{-3} N · s/(m · rad)
$c_{i\theta}$	r_0	μ_k					
10^{-3} N · s/(m · rad)	0.05 m	0.2					

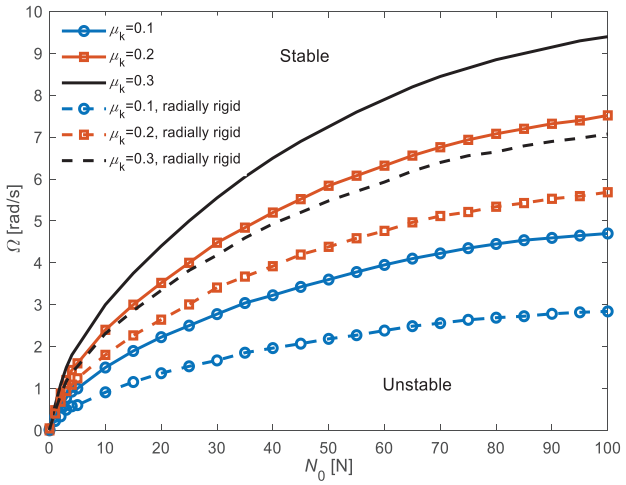

Fig. 5. The stability analysis of the present model and when only the motion in the circumferential direction is considered.

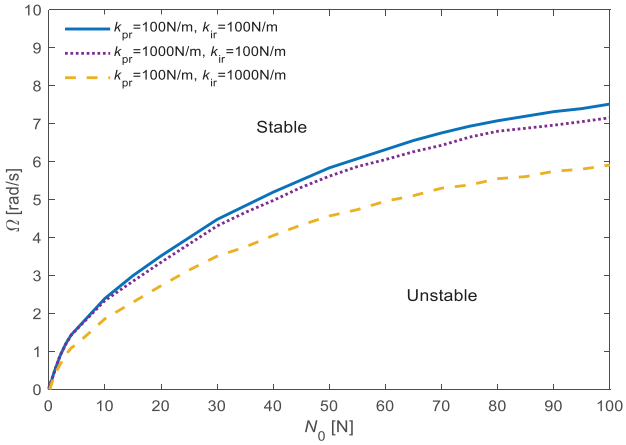

Fig. 6. The stability analysis for different values of stiffnesses in the radial direction.

direction of the pad is considered, i.e., the constraint in the radial direction is assumed to be rigid, are also given. It is observed that the range of operating parameters leading to instability expands with the increase of μ_k. Besides, the comparisons between the results of the present model and the system with only circumferential motion also indicate that the motion in the radial direction is a contributor to the dynamic instability. In Fig. 6, the stability analysis for different values of stiffnesses in the radial direction (k_{pr} and k_{ir}) are given, which demonstrates that k_{ir} has a more significant effect on the dynamic instability of the system than k_{pr}.

IV. STEADY-STATE RESPONSES

A. THE SHOOTING METHOD

The dynamic equations of the system, i.e., equation (1), can be written in the state-space form,

$$\dot{\mathbf{U}} = \mathbf{g}(\mathbf{U}) \tag{14}$$

where $\mathbf{U} = [x,y,\psi,r,\theta,z,\dot{x},\dot{y},\dot{\psi},\dot{r},\dot{\theta},\dot{z}]^{\mathrm{T}}$, and

$$\mathbf{g}(\mathbf{U}) = \begin{bmatrix} \mathbf{0} & \mathbf{I} \\ -\mathbf{M}^{-1}\mathbf{K} & -\mathbf{M}^{-1}\mathbf{C} \end{bmatrix}\mathbf{U} + \begin{bmatrix} \mathbf{0} \\ \mathbf{F}_{\mathrm{con}}(\mathbf{U}) \end{bmatrix} \tag{15}$$

where $\mathbf{F}_{\mathrm{con}}(\mathbf{U}) = [-\mathbf{F}_{\mathrm{f}}\cdot\mathbf{e}_{\mathrm{x}}, -\mathbf{F}_{\mathrm{f}}\cdot\mathbf{e}_{\mathrm{y}}, -R\mathbf{F}_{\mathrm{f}}\cdot\mathbf{e}_{\mathrm{n}}, \mathbf{F}_{\mathrm{f}}\cdot\mathbf{e}_{\mathrm{r}}, \mathbf{F}_{\mathrm{f}}\cdot\mathbf{e}_{\theta}, N-N_0]^{\mathrm{T}}$, $\mathbf{M} = \mathrm{diag}(M,M,I,m,mr_0,m)$, $\mathbf{C} = \mathrm{diag}(c_{\mathrm{dx}},c_{\mathrm{dy}},c_{\mathrm{d}\psi},c_{\mathrm{pr}},c_{\mathrm{p}\theta}r_0,c_{\mathrm{z}})$, and

$$\mathbf{K} = \begin{bmatrix} k_{\mathrm{dx}} & 0 & 0 & 0 & 0 & 0 \\ 0 & k_{\mathrm{dy}} & 0 & 0 & 0 & 0 \\ 0 & 0 & k_{\mathrm{d}\psi} & 0 & 0 & 0 \\ 0 & 0 & 0 & k_{\mathrm{pr}}+\frac{1}{2}k_{\mathrm{ir}} & 0 & -\frac{1}{2}k_{\mathrm{ir}} \\ 0 & 0 & 0 & 0 & k_{\mathrm{p}\theta}+\frac{1}{2}k_{\mathrm{i}\theta} & -\frac{1}{2}k_{\mathrm{i}\theta} \\ 0 & 0 & 0 & -\frac{1}{2}k_{\mathrm{ir}} & -\frac{1}{2}k_{\mathrm{i}\theta}r_0 & \frac{1}{2}(k_{\mathrm{ir}}+k_{\mathrm{i}\theta}) \end{bmatrix}$$

The shooting method aims to find the periodic solution of the system with the governing equations, i.e., equation (14), satisfying the conditions as follows:

$$\mathbf{U}(t+T) = \mathbf{U}(t) \tag{16}$$

where T is the smallest period of the periodic solution. Therefore the periodic solution is found from the following equations,

$$\begin{cases} \dot{\mathbf{U}} = \mathbf{g}(\mathbf{U}) \\ \mathbf{U}(T) = \mathbf{U}(0) = \mathbf{U}_0 \end{cases} \tag{17}$$

where $\mathbf{U}_0$ is the initial condition. Consequently, the unknowns $\mathbf{U}_0$ and T are sought in the shooting method to satisfy the condition of periodicity as,

$$\mathbf{Y}(T,\mathbf{U}_0) = \mathbf{U}(T,\mathbf{U}_0) - \mathbf{U_0} = \mathbf{0} \tag{18}$$

To find the solution of $\mathbf{U}_0$ and T that satisfies the condition equation (18), an iterative Newton-Raphson algorithm [43] is employed, from which the following equation holds for the ith iteration,

$$\mathbf{Y}^i + \left.\frac{\partial \mathbf{Y}}{\partial \mathbf{U}_0}\right|_{(T^i,\mathbf{U}_0{}^i)} \Delta\mathbf{U}_0{}^i + \left.\frac{\partial \mathbf{Y}}{\partial t}\right|_{(T^i,\mathbf{U}_0{}^i)} \Delta T^i + \mathrm{H.O.T.} = 0 \tag{19}$$

where $\Delta^{\mathbf{U}_0} i = \mathbf{U}_0{}^{i+1} - \mathbf{U}_0{}^i$, $\Delta T^i = T^{i+1} - T^i$, H.O.T. are terms with higher order than one. And the partial derivatives $\frac{\partial \mathbf{Y}}{\partial \mathbf{U}_0}$ and $\frac{\partial \mathbf{Y}}{\partial t}$ can be obtained as,

$$\left.\frac{\partial \mathbf{Y}}{\partial \mathbf{U}_0}\right|_{(T^i,\mathbf{U}_0{}^i)} = \left.\frac{\partial \mathbf{U}}{\partial \mathbf{U}_0}\right|_{(T^i,\mathbf{U}_0{}^i)} - \mathbf{I} \tag{20}$$

$$\left.\frac{\partial \mathbf{Y}}{\partial t}\right|_{(T^i,\mathbf{U}_0{}^i)} = \left.\frac{\partial \mathbf{U}}{\partial t}\right|_{(T^i,\mathbf{U}_0{}^i)} = \mathbf{g}(\mathbf{U}(T^i,\mathbf{U}_0{}^i)) \tag{21}$$

The matrix $\frac{\partial \mathbf{U}}{\partial \mathbf{U}_0}$ is obtained by the central difference method [44],

$$\left.\frac{\partial \mathbf{U}}{\partial \mathbf{U}_0}\right|_{(T^i,\mathbf{U}_0{}^i)}(:,k) = \frac{\mathbf{U}(T^i,\mathbf{U}_0{}^i + \delta\boldsymbol{e}_k) - \mathbf{U}(T^i,\mathbf{U}_0{}^i - \delta\boldsymbol{e}_k)}{2\delta} \tag{22}$$

where $\left.\frac{\partial \mathbf{U}}{\partial \mathbf{U}_0}\right|_{(T^i,\mathbf{U}_0{}^i)}(:,k)$ denotes the kth column of $\frac{\partial \mathbf{U}}{\partial \mathbf{U}_0}$, $\mathbf{e}_k$ is a unit vector in which all the elements are zero except the kth element being one. Nevertheless, the number of unknowns is one greater than the number of equations in equation (12), so one more equation for the unknowns is required to obtain the unique solution. The added equation can be chosen as the orthogonality relation between $\mathbf{g}$ and $\Delta\mathbf{U}_0$, i.e.,

$$\mathbf{g}^T(\mathbf{U}(\mathrm{T}^i,\mathbf{U}_0{}^i))\Delta\mathbf{U}_0{}^i = 0 \tag{23}$$

Therefore, the increments $\Delta\mathbf{U}_0{}^i$ and ΔT^i at the ith iteration can be acquired as the solution of equations (19) and (23). And the iteration continues until the criteria of convergence are met as follows:

$$\|\Delta;\mathbf{U}_0{}^i\|/\|\mathbf{U}_0{}^{i+1}\| < \varepsilon_1,\ \ \Delta T^i/T^{i+1} < \varepsilon_2 \tag{24}$$

To initiate the iterative procedure, an estimation of T and $\mathbf{U}_0$, i.e., T^0, $\mathbf{U}_0{}^0$, is made to be the frequency of the unstable mode and the unstable mode of the linearized system, respectively, namely,

$$T^0 = 2\boldsymbol{\pi}/\mathrm{Im}(\lambda) \tag{25}$$

$$\mathbf{U}_0{}^0 = \mathbf{U}_\mathrm{e} + p\mathrm{Re}(\boldsymbol{\Phi}) \tag{26}$$

where λ and $\boldsymbol{\Phi}$ are the eigenvalue and the eigenvector of the unstable mode, respectively; p is a scaling factor, $\mathbf{U}_\mathrm{e} = [\mathbf{u}_\mathrm{e}{}^\mathrm{T}, \mathbf{0}^\mathrm{T}]^\mathrm{T}$ represents the equilibrium point. After obtaining $\mathbf{U}_0$ and T satisfying the condition of periodicity, the integration can be done from 0 to T with the initial value of $\mathbf{U}_0$ to obtain the limit cycle of $\mathbf{U}(t)$.

B. THE TIME INTEGRATION METHOD

To obtain the whole time histories of the dynamic responses of the system, the fourth-order Runge–Kutta method is employed for the integration of dynamic equations in each single state while conditions for state transitions are monitored at each time step. Within the time step in which a state transition happens, the bisection method is used to capture the exact transition time instant. After the transition point, the state changes and the current set of equations of motion is replaced by another one.

The friction force during sticking is not an explicit function of state variables; rather, it can be regarded as an unknown to be determined enforcing the constraint $\|\mathbf{v}_\mathrm{r}\| = 0$. Therefore, to obtain the friction force during sticking, various values of F_fx and F_fy (the components of $\mathbf{F}_\mathrm{f}$ in the x and y directions) are tried when integrating the equations of motion in the state of stick until the values of F_fx and F_fy enabling $\|\mathbf{v}_\mathrm{r}\| = 0$ are found.

C. NUMERICAL EXAMPLES

Suppose the structural parameters of the system are assigned with values as listed in Table I, the steady-state periodic responses when $N_0 = 10\mathrm{N}$, $\Omega = 1\mathrm{rad/s}$ (case 1) and $N_0 = 30\mathrm{N}$, $\Omega = 2\mathrm{rad/s}$ (case 2) are acquired by both the shooting method and the time integration method. δ and p in the shooting method in both cases are chosen as $\delta = 0.01$, $p = 0.8$, and ε_1 and ε_2 have values of 0.01 and 0.001, respectively. It is observed from Figs. 7 and 8 that the periodic responses obtained from the shooting method are in good agreement with those from the time integration method, which demonstrates the accuracy of the shooting method.

In Figs. 9 and 10, the steady state responses for different values of δ and p are exhibited, from which it is observed that the values of δ and p have significant and negligible effects on the convergence of the shooting method to the accurate periodic solutions. Besides, the time costs of the shooting method to obtain the periodic solution for different values of δ and p in the two cases are given in Table II, which shows that both δ and p affects the speed of convergence of the shooting method considerably. Therefore, appropriate values of δ and p should be selected to achieve good accuracy and efficiency of the shooting method, which are $\delta = 0.01$ and $p = 0.8$ in the two given cases. And the computation time to reach the steady-state periodic response by the time integration method is 9.08s for case 1 and 12.16s for case 2, compared with 1.56s for case 1 and 1.97s for case 2 by the shooting method, which demonstrates the great advantage of the shooting method over the conventional time integration method in terms of the computational efficiency.

Next, the characteristics of the steady-state response of the system obtained by the shooting method are analyzed. In Fig. 11, the bifurcation diagram of the system response using N_0 as the control parameter, which show the peak values of the pad's displacement in the circumferential direction, is presented, when $\Omega = 1\mathrm{rad/s}$. It is observed that the system response experiences multiple bifurcations when N_0 varies between 0 and 100N, which can be roughly divided into six intervals with distinct dynamic behaviours that are $[0, 24\mathrm{N}]$, $[25\mathrm{N}, 43\mathrm{N}]$, $[44\mathrm{N}, 61\mathrm{N}]$, $[62\mathrm{N}, 80\mathrm{N}]$, $[81\mathrm{N}, 90\mathrm{N}]$ and $[91\mathrm{N}, 100\mathrm{N}]$. The steady-state responses at $N_0 = 15, 35, 55, 75, 85\mathrm{N}$ that fall into the five different intervals of N_0 are subsequently exhibited in Fig. 12 in terms of time histories, phase plots and frequency spectra

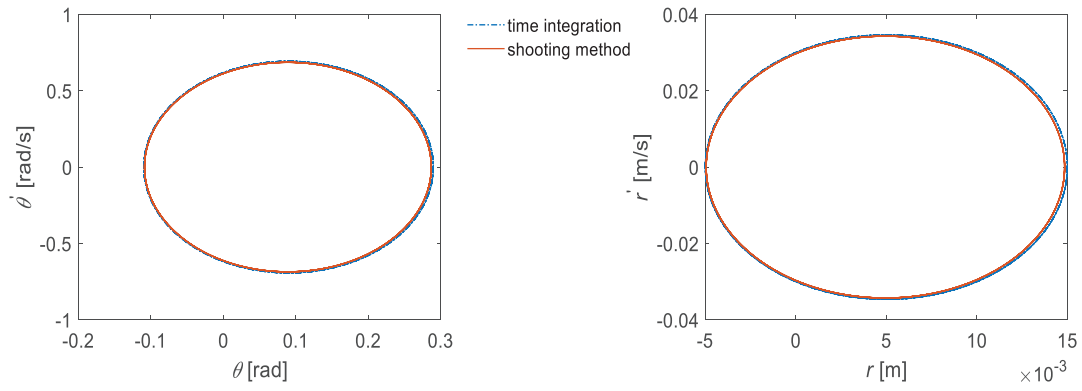

Fig. 7. The steady-state periodic responses when $N_0 = 10\mathrm{N}$, $\Omega = 1\mathrm{rad/s}$ calculated by the shooting method and the time integration method.

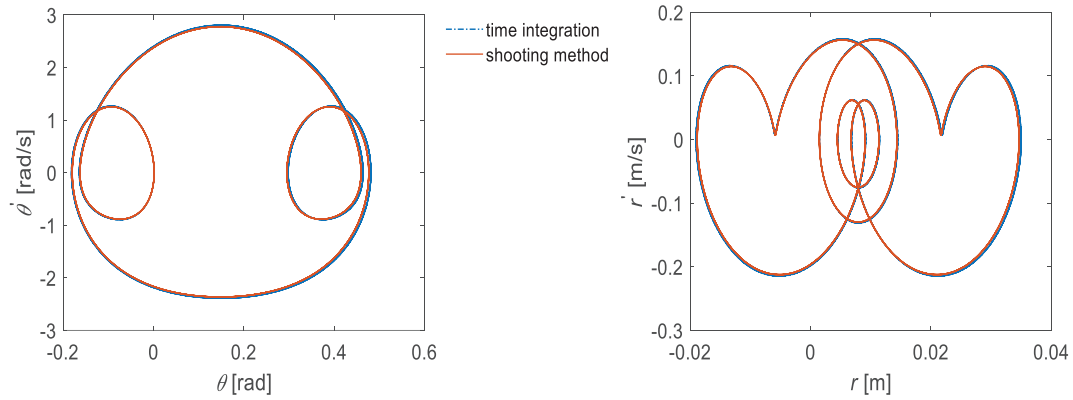

Fig. 8. The steady-state periodic responses when $N_0 = 30\text{N}$, $\Omega = 2\text{rad/s}$ calculated by the shooting method and the time integration method.

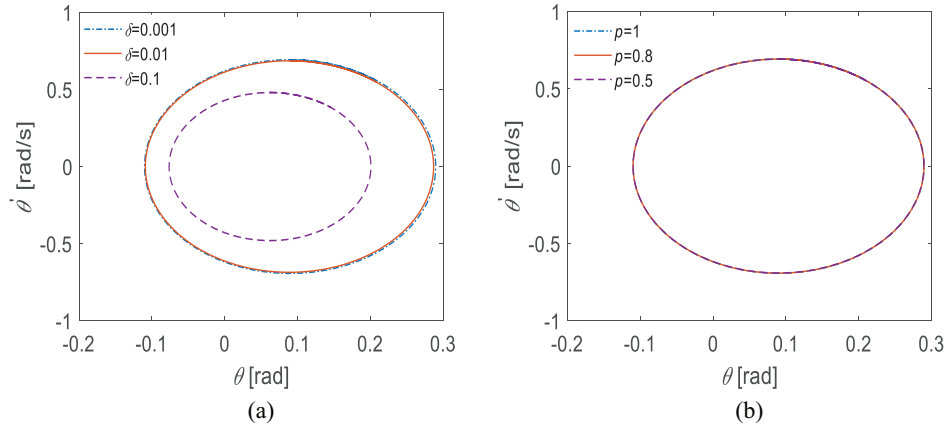

Fig. 9. The steady state responses obtained by the shooting method for different values of δ (a) and p (b) when $N_0 = 10\text{N}$, $\Omega = 1\text{rad/s}$.

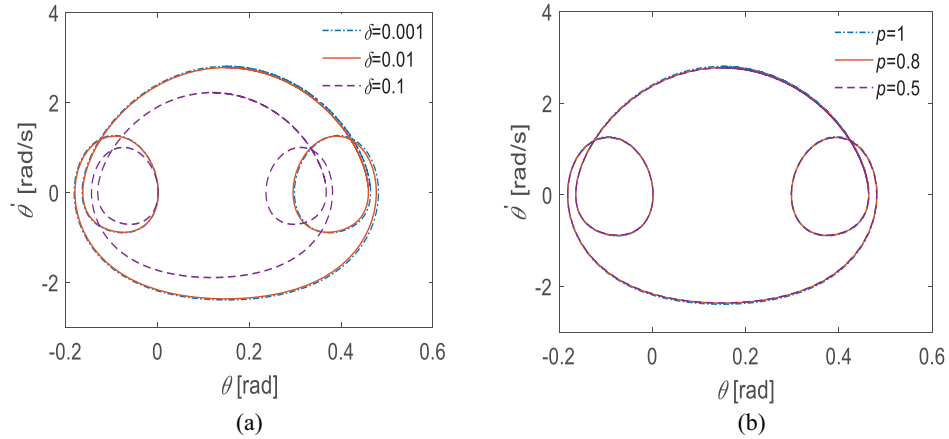

Fig. 10. The steady state responses obtained by the shooting method for different values of δ (a) and p (b) when $N_0 = 30\text{N}$, $\Omega = 2\text{rad/s}$.

of θ. It is seen from Fig. 12(a) that the system response is periodic with almost only one amplitude peak at the frequency of 0.55Hz, indicating the response is nearly harmonic at $N_0 = 15\text{N}$. At $N_0 = 35\text{N}, 55\text{N}, 85\text{N}$, the system responses are also periodic but not harmonic, with the fundamental frequency of 0.48Hz, 0.29Hz, 0.24Hz and corresponding superharmonics, respectively, as shown in Fig. 12(b)–(d). As depicted in Fig. 12(e), the system

Table II. The computation time of the shooting method for different values of δ and p

δ / *p*	0.5 (case1)	0.8 (case1)	1 (case1)	0.5 (case2)	0.8 (case2)	1 (case2)
0.001	29.05s	7.78s	16.03s	35.06s	9.69s	21.25s
0.01	6.67s	1.56s	3.98s	8.02s	1.97s	5.08s
0.1	2.53s	0.49s	1.52s	3.71s	0.79s	1.82s

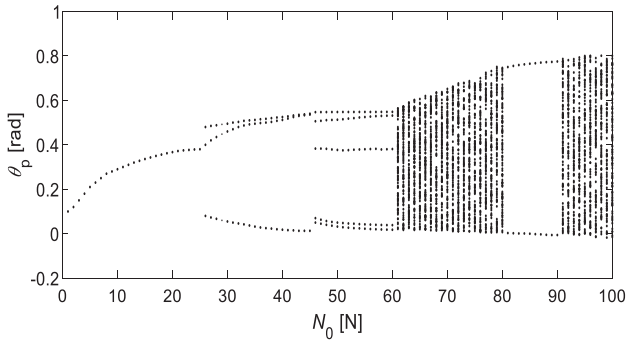

Fig. 11. The bifurcation diagram using N_0 ($\Omega = 1\text{rad/s}$) as the control parameter.

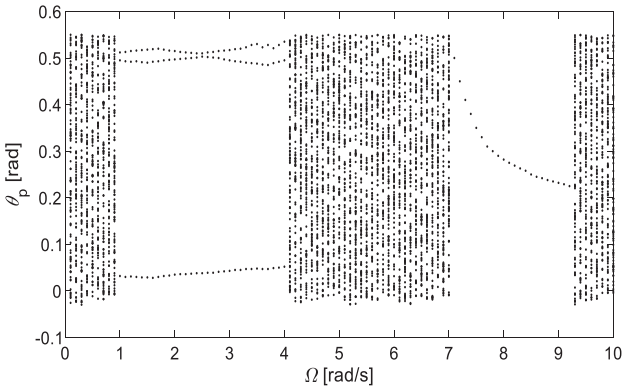

Fig. 13. The bifurcation diagram using Ω ($N_0 = 35\text{N}$) as the control parameter.

response is non-periodic, which can be quasi-periodic or chaotic, at $N_0 = 75\text{N}$. The bifurcation diagram of the system response using Ω as the control parameter is then illustrated in Fig. 13, which also shows rich bifurcational behaviours of the system response.

In contrast, the bifurcation diagrams of the system response using N_0 and Ω as the control parameters when the pad's motion in the radial direction is neglected are presented in Fig. 14. It is clearly seen that there is no bifurcation for the system response with the variation of the control parameters, and the system has periodic vibration all over the ranges of N_0 and Ω. The remarkable differences between the dynamic response of the two system (i.e., with and without the radial motion of the pad) also reflects the significance of the new brake system model in the study of friction-induced vibration in automobile brakes.

Chaotic vibration in the mechanical systems should be avoided because its steady-state behaviour cannot be predicted [44]. In Figs. 15 and 16, the intervals of N_0 ($\Omega = 1\text{rad/s}$) (a) and Ω ($N_0 = 35\text{N}$) in which the proposed system has non-periodic response are for different values of k_{ir} and k_{pr} are depicted. Figure 15 shows that the ranges of

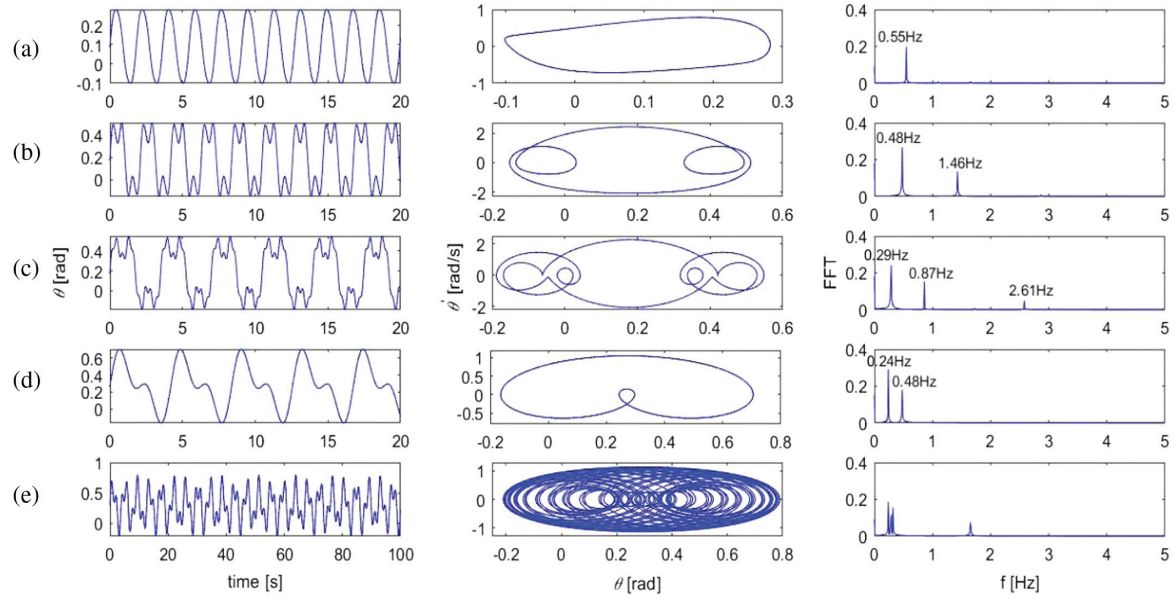

Fig. 12. Time histories, phase plots and frequency spectra of θ at: (a) $N_0 = 15\text{N}$, (b) $N_0 = 35\text{N}$, (c) $N_0 = 55\text{N}$, (d) $N_0 = 85\text{N}$, (e) $N_0 = 75\text{N}$.

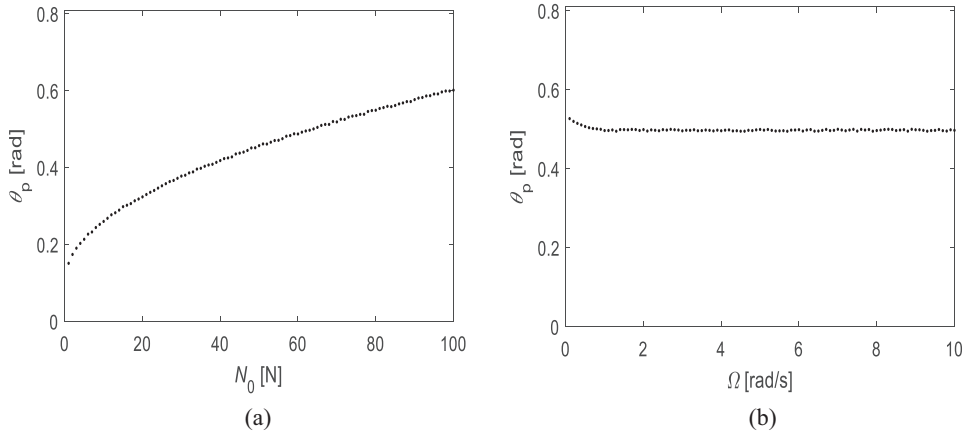

Fig. 14. The bifurcation diagrams using N_0 ($\Omega = 1\text{rad/s}$) (a) and Ω ($N_0 = 35\text{N}$) (b) as the control parameter for the system with the omission of the pad's motion in the radial direction.

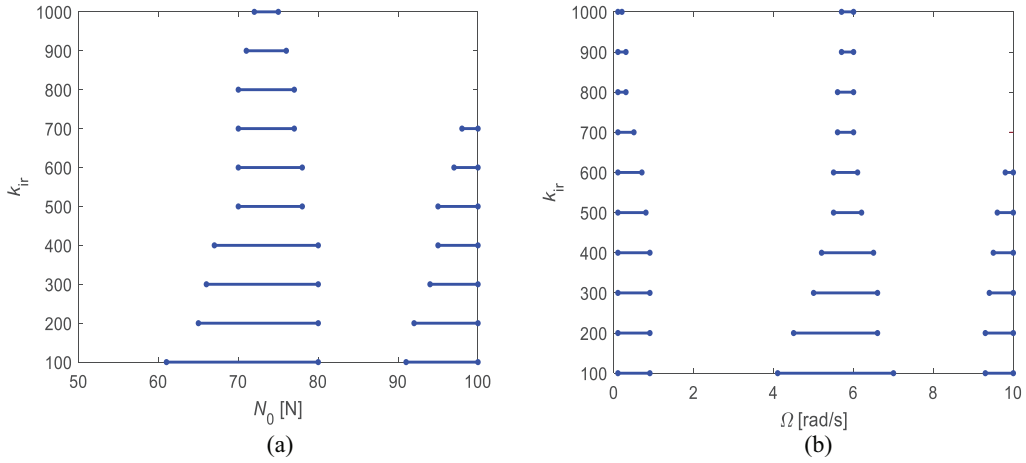

Fig. 15. The ranges of N_0 ($\Omega = 1\text{rad/s}$) (a) and Ω ($N_0 = 35\text{N}$) corresponding to non-periodic response k_{ir}.

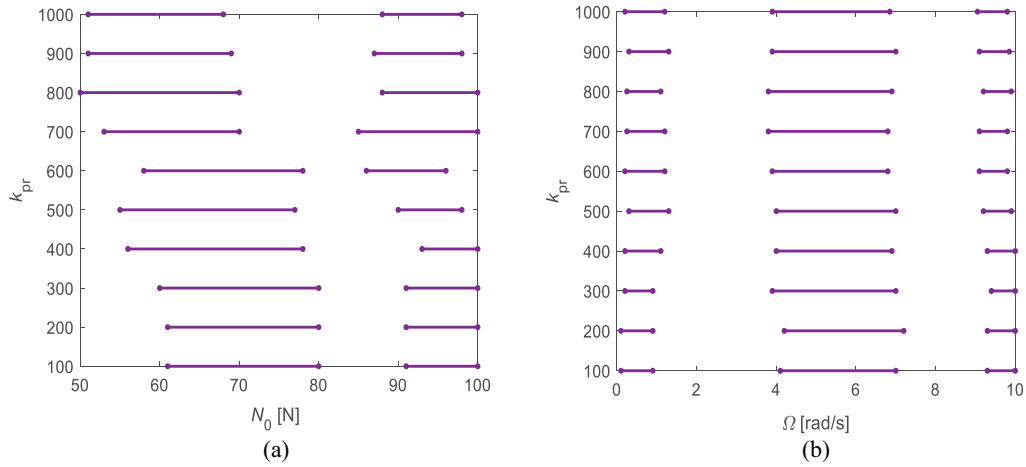

Fig. 16. The ranges of N_0 ($\Omega = 1\text{rad/s}$) (a) and Ω ($N_0 = 35\text{N}$) corresponding to non-periodic response for different values of k_{pr}.

operating parameters corresponding to non-periodic response shrink with the increase of k_{ir}, indicating that k_{ir} is a key parameter for controlling the occurrence of chaotic vibration in the system. Similarly, it can be concluded from Fig. 16 that k_{pr} has little significance on the chaotic vibration.

V. CONCLUSIONS

This paper presents a study of the friction-induced vibration in a new brake system model in which the pad's motions in both radial and circumferential/tangential directions are considered. In the system, the direction of relative motion and friction force is state-dependent rather than always along the circumferential direction. The linear stability analysis and the transient dynamic analysis of the system are performed. For the transient dynamic analysis, two different methods, i.e., the time integration method and the shooting method, are used to calculate steady-state periodic responses of the system. The accuracy and efficiency of the shooting method are examined against the direct time integration. The numerical study in the stability analysis indicates that the integration of the pad's motion in the radial direction contributes to the dynamic instability in the brake system, an k_{ir} (the stiffness of the inclined spring in the radial direction) has more significant effect on the dynamic instability of the system than k_{pr} (the stiffness of the horizontal spring in the radial direction). The numerical results in the transient dynamic analysis demonstrate that there exist rich bifurcation behaviours of the steady-state response in the present brake model with the variations of brake pressure N_0 and disc speed Ω, and k_{ir} is a key parameter for controlling the occurrence of chaotic vibration in the system.

It should be noted that the proposed model in this paper is still a simplified theoretical model of the brake system, and therefore has certain gap from a real brake system. In the future, the finite element model and the test rig of a real automobile brake will be built and investigated to verify and refine the theoretical model.

FUNDING

This work was supported by the Hong Kong Innovation and Technology Commission (Project No. MRP/030/21 under PiH/026/23), The Chinese University of Hong Kong (Project ID: 3134167), and the Research Grants Council (Project No. CUHK14211823) of Hong Kong Special Administrative Region, China.

AUTHOR CONTRIBUTIONS

Ningyu Liu: Conceptualization, Formal analysis, Investigation, Methodology, Validation, Writing-original draft, Writing-review & editing. **Huajiang Ouyang**: Conceptualization, Investigation, Methodology, Writing-review & editing. **Yiqiang Fu**: Formal analysis, Investigation, Validation. **Wei-Hsin Liao**: Funding, Investigation, Project administration, Writing-review & editing.

DATA AVAILABILITY

The datasets generated and analysed during the current study are not publicly available due to the large amount of data but are available from the corresponding authors on reasonable request.

CONFLICT OF INTEREST STATEMENT

The authors have no relevant financial or non-financial interests to disclose.

REFERENCES

[1] A. Papinniemi, J. C. S. Lai, J. Zhao, and L. Loader, "Brake squeal: a literature review," *Appl. Acoust.*, vol. 63, no. 4, pp. 391–400, 2002.

[2] P. A. Meehan and A. C. Leslie, "On the mechanisms, growth, amplitude and mitigation of brake squeal noise," *Mech. Syst. Signal Proc.*, vol. 152, p. 107469, 2021.

[3] N.M. Ghazaly, M. El-Sharkawy, and I. Ahmed, "A review of automotive brake squeal mechanisms," *J. Mech. Des*, vol. 1, no. 1, pp. 5–9, 2014.

[4] R. A. C. Fosberry and Z. Holubecki,*Disc Brake Squeal: Its Mechanism and Suppression*. Lindley: Motor Industry Research Association, 1961.

[5] Y. Yuan, "A study of the effects of negative friction-speed slope on brake squeal," *Proc. ASME. Des. Eng. Tech. Conf. Boston*, vol. 3, pp. 1153–1162, 1995.

[6] C. Gao, D. Kuhlmann-Wilsdorf, and D. D. Makel, "The dynamic analysis of stick-slip motion," *Wear*, vol. 173, no. 1–2, pp. 1–12, 1994.

[7] J. J. Sinou, F. Thouverez, and L. Jezequel, "Analysis of friction and instability by the centre manifold theory for a non-linear sprag-slip model," *J. Sound Vib.*, vol. 265, no. 3, pp. 527–559, 2003.

[8] J. J. Sinou and L. Jézéquel, "Mode coupling instability in friction-induced vibrations and its dependency on system parameters including damping," *Eur. J. Mech. A Solids.*, vol. 26, pp. 106–122, 2007.

[9] H. Ouyang, J. E. Mottershead, M. P. Cartmell, and M. I. Friswell, "Friction-induced parametric resonances in discs: effect of a negative friction-velocity relationship," *J Sound Vib.*, vol. 292, no. 2, pp. 251–263, 1998.

[10] S. N. Chan, J. E. Mottershead, and M. P. Cartmell, "Parametric resonances at subcritical speeds in discs with rotating frictional loads," *Proc. Inst. Mech. Eng., Part C*, vol. 208, no. 6, pp. 417–425, 1994.

[11] D. Lee and A. M. Waas, "Stability analysis of a rotating multi-layer annular plate with a stationary frictional follower load," *Int. J. Mech. Sci.*, vol. 39, no. 10, pp. 1117–1138, 1997.

[12] N. M. Kinkaid, O. M. O'Reilly, and P. Papadopoulos, "On the transient dynamics of a multi-degree-of-freedom friction oscillator: a new mechanism for disc brake noise," *J. Sound Vib.*, vol. 287, no. 4–5, pp. 901–917, 2005.

[13] C. Wu, F. Chen, and X. Long, "The self-excited vibration induced by friction of the shaft-hull coupled system with the water-lubricated rubber bearing and its stick-slip phenomenon," *Ocean Eng.*, vol. 198, p. 107002, 2020.

[14] U. Von Wagner, D. Hochlenert, and P. Hagedorn, "Minimal models for disk brake squeal," *J. Sound Vib.*, vol. 302, no. 3, pp. 527–539, 2007.

[15] J. Kang, "Squeal analysis of gyroscopic disc brake system based on finite element method," *Int. J. Mech. Sci.*, vol. 51, no. 4, pp. 284–294, 2009.

[16] J. Kang, "Automotive brake squeal analysis with rotating finite elements of asymmetric disc in time," *J. Sound Vib.*, vol. 393, pp. 388–400, 2017.

[17] Z. Li, H. Ouyang, and Z. Guan, "Friction-induced vibration of an elastic disc and a moving slider with separation and reattachment," *Nonlinear Dyn.*, vol. 87, no. 2, pp. 1045–1067, 2017.

[18] N. Liu and H. Ouyang, "Friction induced vibration considering multiple types of nonlinearities," *Nonlinear Dyn.*, vol. 102, pp. 2057–2075, 2020.

[19] D. Wei, J. Ruan, W. Zhu, and Z. Kang, "Properties of stability, bifurcation, and chaos of the tangential motion disk brake," *J. Sound Vib.*, vol. 375, pp. 353–365, 2016.

[20] D. Wei, J. Song, Y. Nan, and W. Zhu, "Analysis of the stick-slip vibration of a new brake pad with double-layer structure in automobile brake system," *Mech. Syst. Signal Pr.*, vol. 118, pp. 305–316, 2019.

[21] X. Wang, R. Wang, B. Huang, J. Mo, and H. Ouyang, "A study of effect of various normal force loading forms on frictional stick-slip vibration," *J. Dyn. Monit. Diagn.*, vol. 1, no. 1, pp. 46–55, 2021.

[22] L. C. Bo and D. Pavelescu, "The friction-speed relation and its influence on the critical velocity of stick-slip motion," *Wear*, vol. 82, pp. 277–289, 1982.

[23] S. Andersson, A. Söderberg, and S. Björklund, "Friction models for sliding dry, boundary and mixed lubricated contacts," *Tribol. Int.*, vol. 40, pp. 580–587, 2007.

[24] M. Antali and G. Stepan, "Nonsmooth analysis of three-dimensional slipping and rolling in the presence of dry friction," *Nonlinear Dyn.*, vol. 97, pp. 1799–1817, 2019.

[25] S. Ma and T. Wang, "Planar multiple-contact problems subject to unilateral and bilateral kinetic constraints with static Coulomb friction," *Nonlinear Dyn.*, vol. 94, pp. 99–121, 2018.

[26] J. J. Sinou, O. Chiello, and L. Charroyer, "Non smooth contact dynamics approach for mechanical systems subjected to friction-induced vibration," *Lubr*, vol. 7, no. 7, p. 59, 2019.

[27] L. Charroyer, O. Chiello, and J. J. Sinou, "Parametric study of the mode coupling instability for a simple system with planar or rectilinear friction," *J. Sound Vib.*, vol. 384, pp. 94–112, 2016.

[28] C. H. Menq, P. Chidamparam, and J. H. Griffin, "Friction damping of two-dimensional motion and its application in vibration control," *J. Sound Vib.*, vol. 144, no. 3, pp. 427–447, 1991.

[29] C. Weiss, M. Merlock, and N. Hoffmann, "Friction induced dynamics of ball joints: Instability and post bifurcation behavior," *Eur. J. Mech. A Solids.*, vol. 45, pp. 161–173, 2014.

[30] F. Massi, L. Baillet, O. Giannini, and A. Sestieri, "Brake squeal: linear and nonlinear numerical approaches," *Mech. Syst. Signal Pr.*, vol. 21, no. 6, pp. 2374–2393, 2007.

[31] B. Hervé, J. J. Sinou, H. Mahé, and L. Jézéquel, "Analysis of squeal noise and mode coupling instabilities including damping and gyroscopic effects," *Eur. J. Mech. A Solids.*, vol. 27, no. 2, pp. 141–160, 2008.

[32] H. Celikag, E. Ozturk, and N. D. Sims, "Can mode coupling chatter happen in milling?" *Int. J. Mach. Tool.*, vol. 165, p. 103738, 2021.

[33] O. Gienke, Z. Pan, L. Yuan, T. Lepper, and S. Van Duin, "Mode coupling chatter prediction and avoidance in robotic machining process," *Int. J. Adv. Manuf.*, vol. 104, pp. 2103–2116, 2019.

[34] G. Tuzzi, C. W. Schwingshackl, and J. S. Green, "Study of coupling between shaft bending and disc zero nodal diameter modes in a flexible shaft-disc assembly," *J. Sound Vib.*, vol. 479, pp. 115362, 2020.

[35] N. Liu and H. Ouyang, "Friction-induced vibration of a slider on an elastic disc spinning at variable speeds," *Nonlinear Dyn.*, vol. 98, pp. 39–60, 2019.

[36] H. Hu, A. Batou, H. Ouyang, and N. Liu, "Friction-induced planar vibration of a two-rigid-disc system with a finite contact area subjected to uncertain friction," *Nonlinear Dyn.*, vol. 111, pp. 18677–18696, 2023.

[37] N. Liu and H. Ouyang, "Friction-induced planar vibration of two rigid plates," *Appl. Math. Model.*, vol. 109, pp. 613–628, 2022.

[38] Z. Zhang, S. Oberst, and J. C. S. Lai, "A non-linear friction work formulation for the analysis of self-excited vibrations," *J. Sound Vib.*, vol. 443, pp. 328–340, 2019.

[39] N. Coudeyras, J. J. Sinou, and S. Nacivet, "A new treatment for predicting the self-excited vibrations of nonlinear systems with frictional interfaces: the constrained harmonic balance method with application to disc brake squeal," *J. Sound Vib.*, vol. 319, no. 3–5, pp. 1175–1199, 2009.

[40] L. C. Young, "Orthogonal collocation revisited," *Comput. Method Appl. M.*, vol. 345, pp. 1033–1076, 2019.

[41] B. S. Attili and M. I. Syam, "Efficient shooting method for solving two point boundary value problems," *Chaos Soliton Fract.*, vol. 35, no. 5, pp. 895–903, 2008.

[42] F. Marques, P. Flores, J. P. Claro, and H. M. Lankarani, "A survey and comparison of several friction force models for dynamic analysis of multibody mechanical systems," *Nonlinear Dyn.*, vol. 86, no. 3, pp. 1407–1443, 2016.

[43] A. Ben-Israel, "A Newton-Raphson method for the solution of systems of equations," *J. Math. Anal. Appl.*, vol. 15, no. 2, pp. 243–252, 1966.

[44] S. Oberst and J. C. S. Lai, "Chaos in brake squeal noise," *J. Sound Vib.*, vol. 330, no. 5, pp. 955–975, 2011.

APPENDIX

From derivation, the damping matrix $\mathbf{C}_\mathrm{L}$ is symmetric, while the stiffness matrix $\mathbf{K}_\mathrm{L}$ is non-symmetric, and the entries of $\mathbf{C}_\mathrm{L}$ and $\mathbf{K}_\mathrm{L}$ are obtained as follows:

for $\mathbf{C}_\mathrm{L}$,

$$\mathbf{C}_\mathrm{L}(1,1) = c_\mathrm{dx} - \frac{\mu_\mathrm{k} k_\mathrm{z} z_e v_{ye}^2}{(v_{xe}^2 + v_{ye}^2)^{3/2}}, \tag{A.1}$$

$$\mathbf{C}_\mathrm{L}(1,2) = \frac{\mu_\mathrm{k} k_\mathrm{z} z_e v_{xe} v_{ye}}{(v_{xe}^2 + v_{ye}^2)^{3/2}}, \tag{A.2}$$

$$\mathbf{C}_\mathrm{L}(1,3) = \frac{\mu_\mathrm{k} k_\mathrm{z} z_e [v_{ye}^2((r_0 + r_e)\sin(\theta_0 + \theta_e) - y_e) - v_{xe} v_{ye}(x_e - (r_0 + r_e)\cos(\theta_0 + \theta_e))]}{(v_{xe}^2 + v_{ye}^2)^{3/2}}, \tag{A.3}$$

$$\mathbf{C}_\mathrm{L}(1,4) = \frac{\mu_\mathrm{k} k_\mathrm{z} z_e [v_{ye}^2 \cos(\theta_0 + \theta_e) - v_{xe} v_{ye} \sin(\theta_0 + \theta_e)]}{(v_{xe}^2 + v_{ye}^2)^{3/2}}, \tag{A.4}$$

$$\mathbf{C}_\mathrm{L}(1,5) = \frac{\mu_\mathrm{k} k_\mathrm{z} z_e (r_0 + r_e)[v_{ye}^2 \sin(\theta_0 + \theta_e) + v_{xe} v_{ye} \cos(\theta_0 + \theta_e)]}{(v_{xe}^2 + v_{ye}^2)^{3/2}}, \tag{A.5}$$

$$\mathbf{C}_\mathrm{L}(2,2) = c_\mathrm{dy} - \frac{\mu_\mathrm{k} k_\mathrm{z} z_e v_{xe}^2}{(v_{xe}^2 + v_{ye}^2)^{3/2}}, \tag{A.6}$$

$$\mathbf{C}_\mathrm{L}(2,3) = \frac{\mu_\mathrm{k} k_\mathrm{z} z_e [v_{xe}^2(x_e - (r_0 + r_e)\cos(\theta_0 + \theta_e)) - v_{xe} v_{ye}((r_0 + r_e)\sin(\theta_0 + \theta_e) - y_e)]}{(v_{xe}^2 + v_{ye}^2)^{3/2}}, \tag{A.7}$$

$$\mathbf{C}_\mathrm{L}(2,4) = \frac{\mu_\mathrm{k} k_\mathrm{z} z_e [v_{xe}^2 \sin(\theta_0 + \theta_e) - v_{xe} v_{ye} \cos(\theta_0 + \theta_e)]}{(v_{xe}^2 + v_{ye}^2)^{3/2}}, \tag{A.8}$$

$$\mathbf{C}_\mathrm{L}(2,5) = \frac{\mu_\mathrm{k} k_\mathrm{z} z_e (r_0 + r_e)[v_{xe}^2 \cos(\theta_0 + \theta_e) + v_{xe} v_{ye} \sin(\theta_0 + \theta_e)]}{(v_{xe}^2 + v_{ye}^2)^{3/2}}, \tag{A.9}$$

$$\mathbf{C}_\mathrm{L}(3,3) = c_{\mathrm{d}\psi}, \tag{A.10}$$

$$\mathbf{C}_\mathrm{L}(3,4) = \frac{\mu_\mathrm{k} k_\mathrm{z} z_e [v_{xe}^2 \sin(\theta_0 + \theta_e) - v_{ye}^2 \cos(\theta_0 + \theta_e)]}{(v_{xe}^2 + v_{ye}^2)^{1/2}}, \tag{A.11}$$

$$\mathbf{C}_\mathrm{L}(4,4) = c_\mathrm{pr} + \frac{\mu_\mathrm{k} k_\mathrm{z} z_e [v_{xe}^2 \sin^2(\theta_0 + \theta_e) + v_{ye}^2 \cos^2(\theta_0 + \theta_e) - 2 v_{xe} v_{ye} \sin(\theta_0 + \theta_e)\cos(\theta_0 + \theta_e)]}{(v_{xe}^2 + v_{ye}^2)^{3/2}}, \tag{A.12}$$

$$\mathbf{C}_\mathrm{L}(5,5) = r_0 c_{\mathrm{p}\theta} + \frac{\mu_\mathrm{k} k_\mathrm{z} z_e [v_{xe}^2 \cos^2(\theta_0 + \theta_e) + v_{ye}^2 \sin^2(\theta_0 + \theta_e) + 2 v_{xe} v_{ye} \sin(\theta_0 + \theta_e)\cos(\theta_0 + \theta_e)]}{(v_{xe}^2 + v_{ye}^2)^{3/2}}, \tag{A.13}$$

$$\mathbf{C}_\mathrm{L}(6,6) = c_\mathrm{z}, \tag{A.14}$$

$$\mathbf{C}_\mathrm{L}(1,6) = \mathbf{C}_\mathrm{L}(2,6) = \mathbf{C}_\mathrm{L}(3,5) = \mathbf{C}_\mathrm{L}(3,6) = \mathbf{C}_\mathrm{L}(4,5) = \mathbf{C}_\mathrm{L}(4,6) = \mathbf{C}_\mathrm{L}(5,6) = 0, \tag{A.15}$$

$$\mathbf{C}_{\mathrm{L}}(i,j) = \mathbf{C}_{\mathrm{L}}(j,i) \qquad (2 \le i \le 6,\ 1 \le j \le 5,\ i > j), \tag{A.16}$$

for $\mathbf{K}_{\mathrm{L}}$,

$$\mathbf{K}_{\mathrm{L}}(1,1) = k_{\mathrm{dx}} - \frac{\mu_{\mathrm{k}} k_{\mathrm{z}} z_e \Omega v_{xe} v_{ye}}{(v_{xe}^2 + v_{ye}^2)^{3/2}}, \tag{A.17}$$

$$\mathbf{K}_{\mathrm{L}}(1,2) = -\frac{\mu_{\mathrm{k}} k_{\mathrm{z}} z_e \Omega v_{ye}^2}{(v_{xe}^2 + v_{ye}^2)^{3/2}}, \tag{A.18}$$

$$\mathbf{K}_{\mathrm{L}}(1,4) = \frac{\mu_{\mathrm{k}} k_{\mathrm{z}} z_e \Omega v_{ye} (v_{ye}\sin(\theta_0 + \theta_e) + v_{xe}\cos(\theta_0 + \theta_e))}{(v_{xe}^2 + v_{ye}^2)^{3/2}}, \tag{A.19}$$

$$\mathbf{K}_{\mathrm{L}}(1,5) = \frac{\mu_{\mathrm{k}} k_{\mathrm{z}} z_e \Omega v_{ye} (r_0 + r_e)(v_{ye}\cos(\theta_0 + \theta_e) - v_{xe}\sin(\theta_0 + \theta_e))}{(v_{xe}^2 + v_{ye}^2)^{3/2}}, \tag{A.20}$$

$$\mathbf{K}_{\mathrm{L}}(1,6) = \frac{\mu_{\mathrm{k}} k_{\mathrm{z}} v_{xe}}{(v_{xe}^2 + v_{ye}^2)^{1/2}}, \tag{A.21}$$

$$\mathbf{K}_{\mathrm{L}}(2,1) = \frac{\mu_{\mathrm{k}} k_{\mathrm{z}} z_e \Omega v_{xe}^2}{(v_{xe}^2 + v_{ye}^2)^{3/2}}, \tag{A.22}$$

$$\mathbf{K}_{\mathrm{L}}(2,2) = k_{\mathrm{dy}} + \frac{\mu_{\mathrm{k}} k_{\mathrm{z}} z_e \Omega v_{xe} v_{ye}}{(v_{xe}^2 + v_{ye}^2)^{3/2}}, \tag{A.23}$$

$$\mathbf{K}_{\mathrm{L}}(2,4) = -\frac{\mu_{\mathrm{k}} k_{\mathrm{z}} z_e \Omega v_{xe} (v_{ye}\sin(\theta_0 + \theta_e) + v_{xe}\cos(\theta_0 + \theta_e))}{(v_{xe}^2 + v_{ye}^2)^{3/2}}, \tag{A.24}$$

$$\mathbf{K}_{\mathrm{L}}(2,5) = \frac{\mu_{\mathrm{k}} k_{\mathrm{z}} z_e \Omega (r_0 + r_e) v_{xe} (v_{xe}\sin(\theta_0 + \theta_e) - v_{ye}\cos(\theta_0 + \theta_e))}{(v_{xe}^2 + v_{ye}^2)^{3/2}}, \tag{A.25}$$

$$\mathbf{K}_{\mathrm{L}}(2,6) = \frac{\mu_{\mathrm{k}} k_{\mathrm{z}} v_{ye}}{(v_{xe}^2 + v_{ye}^2)^{1/2}}, \tag{A.26}$$

$$\mathbf{K}_{\mathrm{L}}(3,1) = -\frac{\mu_{\mathrm{k}} k_{\mathrm{z}} z_e (2v_{ye} + \Omega x_e)}{(v_{xe}^2 + v_{ye}^2)^{1/2}}, \tag{A.27}$$

$$\mathbf{K}_{\mathrm{L}}(3,2) = \frac{\mu_{\mathrm{k}} k_{\mathrm{z}} z_e (2v_{xe} - \Omega y_e)}{(v_{xe}^2 + v_{ye}^2)^{1/2}}, \tag{A.28}$$

$$\mathbf{K}_{\mathrm{L}}(3,3) = k_{\mathrm{d}\psi}, \tag{A.29}$$

$$\mathbf{K}_{\mathrm{L}}(3,4) = \frac{\mu_{\mathrm{k}} k_{\mathrm{z}} z_e (2v_{ye}\cos(\theta_0 + \theta_e) - 2v_{xe}\sin(\theta_0 + \theta_e) - \Omega(r_0 + r_e))}{(v_{xe}^2 + v_{ye}^2)^{1/2}}, \tag{A.30}$$

$$\mathbf{K}_{\mathrm{L}}(3,5) = -\frac{2\mu_{\mathrm{k}} k_{\mathrm{z}} z_e (r_0 + r_e)(v_{xe}\cos(\theta_0 + \theta_e) + v_{ye}\sin(\theta_0 + \theta_e))}{(v_{xe}^2 + v_{ye}^2)^{1/2}}, \tag{A.31}$$

$$\mathbf{K}_{\mathrm{L}}(3,6)=\frac{\mu_{\mathrm{k}}k_{\mathrm{z}}(v_{xe}^2+v_{ye}^2)^{1/2}}{\Omega}, \tag{A.32}$$

$$\mathbf{K}_{\mathrm{L}}(4,1)=\frac{\mu_{\mathrm{k}}k_{\mathrm{z}}z_e\Omega v_{xe}(v_{xe}\sin(\theta_0+\theta_e)-v_{ye}\cos(\theta_0+\theta_e))}{(v_{xe}^2+v_{ye}^2)^{3/2}}, \tag{A.33}$$

$$\mathbf{K}_{\mathrm{L}}(4,2)=\frac{\mu_{\mathrm{k}}k_{\mathrm{z}}z_e\Omega v_{ye}(v_{xe}\sin(\theta_0+\theta_e)-v_{ye}\cos(\theta_0+\theta_e))}{(v_{xe}^2+v_{ye}^2)^{3/2}}, \tag{A.34}$$

$$\mathbf{K}_{\mathrm{L}}(4,4)=k_{\mathrm{pr}}+\frac{1}{2}k_{\mathrm{ir}}+\frac{\mu_{\mathrm{k}}k_{\mathrm{z}}z_e(v_{xe}\cos(\theta_0+\theta_e)+v_{ye}\sin(\theta_0+\theta_e))}{(v_{xe}^2+v_{ye}^2)^{3/2}}, \tag{A.35}$$

$$\mathbf{K}_{\mathrm{L}}(4,5)=\frac{\mu_{\mathrm{k}}k_{\mathrm{z}}z_e\Omega(r_0+r_e)(v_{ye}\cos(\theta_0+\theta_e)-v_{xe}\sin(\theta_0+\theta_e))}{(v_{xe}^2+v_{ye}^2)^{1/2}}, \tag{A.36}$$

$$\mathbf{K}_{\mathrm{L}}(4,6)=-\frac{1}{2}k_{\mathrm{ir}}+\frac{\mu_{\mathrm{k}}k_{\mathrm{z}}(v_{xe}\cos(\theta_0+\theta_e)+v_{ye}\sin(\theta_0+\theta_e))}{(v_{xe}^2+v_{ye}^2)^{1/2}}, \tag{A.37}$$

$$\mathbf{K}_{\mathrm{L}}(5,1)=\frac{\mu_{\mathrm{k}}k_{\mathrm{z}}z_e\Omega v_{xe}^2\sin^2(\theta_0+\theta_e)}{(v_{xe}^2+v_{ye}^2)^{3/2}}, \tag{A.38}$$

$$\mathbf{K}_{\mathrm{L}}(5,2)=\frac{\mu_{\mathrm{k}}k_{\mathrm{z}}z_e\Omega v_{ye}^2\cos^2(\theta_0+\theta_e)}{(v_{xe}^2+v_{ye}^2)^{3/2}}, \tag{A.39}$$

$$\mathbf{K}_{\mathrm{L}}(5,4)=\frac{\mu_{\mathrm{k}}k_{\mathrm{z}}z_e(2v_{xe}\cos(\theta_0+\theta_e)+2v_{ye}\sin(\theta_0+\theta_e)-\Omega(r_0+r_e))}{(v_{xe}^2+v_{ye}^2)^{3/2}}, \tag{A.40}$$

$$\mathbf{K}_{\mathrm{L}}(5,5)=r_0(k_{\mathrm{pr}}+\frac{1}{2}k_{\mathrm{ir}})-\frac{2\mu_{\mathrm{k}}k_{\mathrm{z}}z_e\Omega(r_0+r_e)(v_{xe}\cos(\theta_0+\theta_e)+v_{ye}\sin(\theta_0+\theta_e))}{(v_{xe}^2+v_{ye}^2)^{1/2}}, \tag{A.41}$$

$$\mathbf{K}_{\mathrm{L}}(5,6)=-\frac{1}{2}k_{\mathrm{i}\theta}+\frac{\mu_{\mathrm{k}}k_{\mathrm{z}}(-v_{xe}\sin(\theta_0+\theta_e)+v_{ye}\cos(\theta_0+\theta_e))}{\Omega}, \tag{A.42}$$

$$\mathbf{K}_{\mathrm{L}}(6,4)=-\frac{1}{2}k_{\mathrm{ir}}-\frac{1}{2}k_{\mathrm{i}\theta}\theta_e, \tag{A.43}$$

$$\mathbf{K}_{\mathrm{L}}(6,5)=-\frac{1}{2}k_{\mathrm{i}\theta}r_e, \tag{A.44}$$

$$\mathbf{K}_{\mathrm{L}}(6,6)=\frac{1}{2}(k_{\mathrm{ir}}+k_{\mathrm{i}\theta})+k_{\mathrm{z}}, \tag{A.45}$$

$$\mathbf{K}_{\mathrm{L}}(1,3)=\mathbf{K}_{\mathrm{L}}(2,3)=\mathbf{K}_{\mathrm{L}}(4,3)=\mathbf{K}_{\mathrm{L}}(5,3)=\mathbf{K}_{\mathrm{L}}(6,1)=\mathbf{K}_{\mathrm{L}}(6,2)=\mathbf{K}_{\mathrm{L}}(6,3)=0, \tag{A.46}$$

where $v_{xe}=\Omega(r_0+r_e)\sin(\theta_0+\theta_e)-\Omega y_e$, $v_{ye}=-\Omega(r_0+r_e)\cos(\theta_0+\theta_e)+\Omega x_e$.